[redacted]

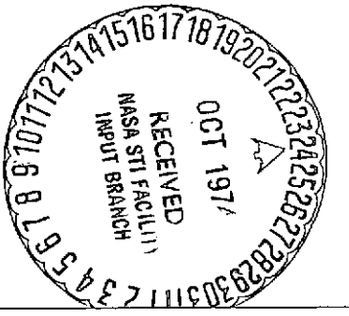

Lockheed

MISSILES & SPACE COMPANY, INC.

A SUBSIDIARY OF LOCKHEED AIRCRAFT CORPORATION

SUNNYVALE, CA

Enclosure to
LMSC D404808

Final Report

COORDINATED ROCKET AND SATELLITE OBSERVATIONS OF THE SOLAR CORONA

July 1974

Prepared For

NATIONAL AERONAUTICS AND SPACE ADMINISTRATION
Washington, D.C. 20546

Contract NASW-2589

Principal Investigator: Dr. W. T. Zaumen

Radiation Physics Laboratory
Lockheed Palo Alto Research Laboratory
3251 Hanover Street
Palo Alto, California 94304

COORDINATED ROCKET AND SATELLITE OBSERVATIONS OF THE SOLAR CORONA

INTRODUCTION

The purpose of this research program is to study coronal condensations associated with active regions by comparing their x-ray and EUV line intensities. The EUV line measurements were made with the OSO-H satellite, and the x-ray measurements were made with an ATM support rocket, Aerobee 26.002. The rocket x-ray detection system is considerably more sensitive than the OSO-H x-ray system. This increased sensitivity gives the justification for a coordinated observing program.

The data obtained from these observations are used to find the emission measure distribution at low temperatures ($\sim 1 \times 10^6$ K to 5×10^6 K). Studies by Parkinson (1971) and Batstone et al. (1970) indicate that the low temperature behavior of the emission measureme is of physical interest. It has become apparent recently that determining the emission measure from line spectra requires data with good statistics on a large number of spectral lines. The temperatures over which these lines are observed should furthermore cover a broad range of temperatures with each line sensitive to as narrow a range of temperatures as practical.

DATA:

Crystal Spectrometers on Aerobee 26.002 measured the line intensities for OVII at 21.60 Å, OVIII at 18.97 Å, Fe XVII at 15.01 Å, and Ne IX at 13.45 Å. In additional proportional counter measurements provide some information on line strengths for Mg XI at 9.2 Å and Si XIII at 11.6 Å. The field of view of the spectrometer was .6 arcmin for one system which measured OVII, OVIII, Ne IX and Fe XVII lines, and 1.5 arcmin for another which measured Fe XVII and OVII alone. The proportional counter field of view was 0.6 arcmin.

The OSO-H satellite over a several hour period before and after the rocket flight measured the line intensities of Fe IX at 171.074 Å, Fe IX at 188.22 Å, Fe XII at 195.14 Å, and Fe XIII at 203.84 Å. During each pass, a different

line was measured and measurements were also switched between the two active regions observed by the rocket.

Figure 1 shows the regions of the sun observed by Aerobee 26.002. Table 1 contains the rocket line intensity data for each of the 16 points on the sun which were observed. For each orbit, these points have slightly different OSO-H spacecraft coordinates. The relation between Table 2 shows the OSO-H coordinates for each of these points for each orbit of the satellite. The method for comparing these data, then, is for each OSO-H orbit to sum the OSO-H data over all points (for that orbit) within the field of view for a given rocket measurement.

DATA ANALYSIS:

Batstone et al. (1970) give the following expression for the line intensity:

$$E_i = 8 \times 10^{-43} \, gfA_z \int G(T_e) \, N_e^2 \, dV \, dT_e \qquad (1)$$

where g is the temperature averaged Gaunt factor, f the oscillator strength, A_z the coronal abundance relative to Hydrogen of the element z, N_e the electron density, and E_i, the energy flux. All quantities are in cgs units. $G(T_e)$ is defined as

$$G(T_e) = T_e^{-0.5} \, A_{z_i} \exp(- h\nu_z / hT_e) \quad ,$$

where A_{z_i} is the fractional abundance of element z in ionization state i at temperature T_e. If we represent the equation (1) by a matrix equation we obtain

$$E_i = \sum_j B_{ij} \left[\int N_e^2 \, dV\right]_{T_{e_i}} \qquad (2)$$

where

$$B_{ij} = 8 \times 10^{43} \, gfA_z \, G(T_{e_j}) \qquad (3)$$

Values for A_{z_i} are given by Jordan (1969, 1970). Atomic abundances are given

by Withbroe (1971), and oscillator strengths are obtained from Mewe (1972) and Fawcett et al. (1968). These results are summarized in Table 3.

Instead of attempting a least squares fit to the data in order to determine the emission measure distribution as Batstone does, where the emission measure at each temperature is a free parameter, we use the finite difference approximation (Eq. 3) and perform a least squares fit with a 4 parameter model for $[\int N_e^2 \, dV]_{T_{e_i}}$. Batstone could not obtain a physically reasonable emission measurer without constraining the emission measure to lie within certain bounds. We take this as an indication that line intensity data is not good enough to uniquely determine an emission measure distribution from the data alone. We therefore feel that fitting the data with a reasonable model is a better approach. Such a model has been proposed by Walker (1971) and gives

$$S(T) = C10^{-T_2/T_1}\left[1 + 1.1515(T_2-T_0)/T_1 - 1.1515B(T-T_0)^2/T_1(T_2-T_0)\right] \qquad 1 \times 10^6\ ^\circ K < T < T_0$$

$$S(T) = C10^{-T_2/T_1}\left[1 + 1.1515(T_2-T_0)/T_1 - 1.1515(T-T_0)^2/T_1(T_2-T_0)\right] \qquad T_0 < T < T_2$$

$$S(T) = C10^{-T/T_1} \qquad T > T_2 \quad , \qquad (4)$$

where the parameter B is selected so that $S(1 \times 10^6)/S(T_0) = 0.4$ and T_0 is the most probable coronal temperature.

A program has been written for doing this least squares fit; however, final calculations have not yet been performed as the OSO-H group at the Goddard Space Flight Center is finishing the absolute calibration of their instrument. This data will improve the accuracy of our emission measure fit considerably, as we can then compare the EUV and x-ray data directly.

REFERENCES

Batstone, R.M., Evans, J., Parkinson, J.H. and Pounds, J.A.; 1970, Solar Phys. 13, 389.

Fawcett, ; 1968, J. Phys. B., (Proc. Phys. Soc.) Ser 2, I, 295.

Jordan, C.; 1970, M.N.R.A.S. 148, 17

Jordan, C.; 1969, M.N.R.A.S. 142, 501.

Meve, R.; 1972, Solar Phys. 22, 459.

Parkinson, J.H.; 1971, Thesis, University of Leicester, Leicester, England.

Walker, A.B.C.; 1971, "Symposium on Laboratory and Astrophysical Plasmas," I.A.U.

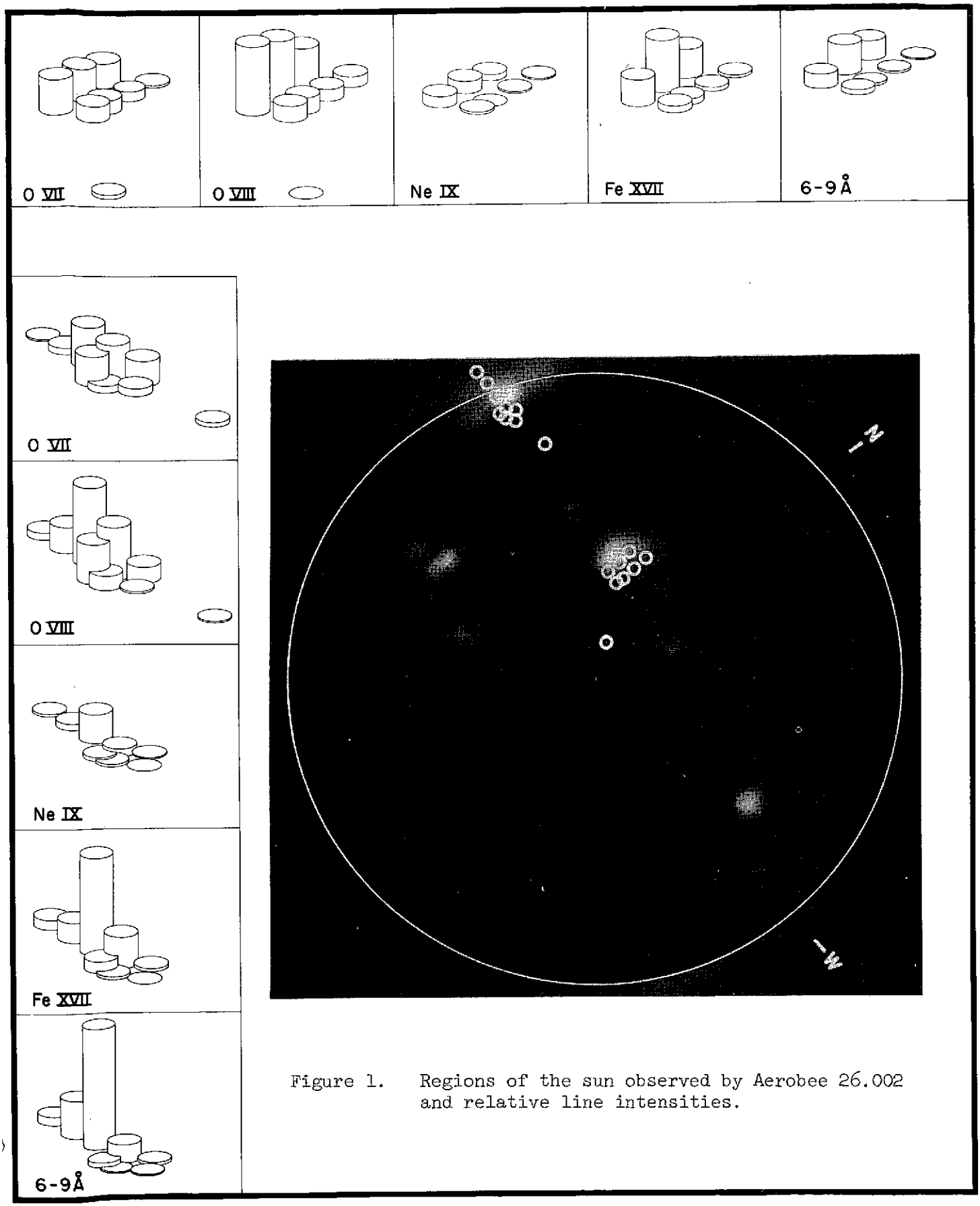

Figure 1. Regions of the sun observed by Aerobee 26.002 and relative line intensities.

TABLE 1

Line Strengths for Aerobee 26.002 Data

Rocket Position	O VII 10^{-6} ergs km^2/sec	O VIII 10^{-6} ergs km^2/sec	Fe XVII 10^{-6} ergs km^2/sec	Ne IX 10^{-6} ergs km^2/sec
1	60.2	92.1	84.2	17.7
2	65.6	139.5	133.7	41.4
3	67.1	156.0	72.9	34.9
4	76.4	159.7	82.5	33.3
5	3.9	22.9	8.2	2.7
6	19.3	27.2	11.7	4.8
7	27.8	36.2	16.5	1.1
8	32.4	37.3	21.3	5.4
	9.3	1.6	0	0
9	51.7	38.3	10.9	3.2
10	43.9	30.9	9.5	7.0
11	60.2	96.4	38.2	11.8
12	76.4	133.1	92.0	26.9
13	16.2	5.3	1.3	1.1
14	88.7	189.6	281.2	90.9
15	31.6	77.2	65.1	21.5
16	0	0	67.3	25.3

TABLE 2

OSO-H Coordinates (Azimuth, Elevation) for Rocket Positions

Rocket Position	Orbit No. 9646	9647	9652
1	(62.12, 65.03)	(62.12, 65.01)	(62.11, 64.98)
2	(51.98, 64.49)	(51.98, 64.44)	(51.98, 64.27)
3	(53.63, 63.16)	(53.64, 63.12)	(53.66, 62.97)
4	(54.65, 64.07)	(54.65, 64.03)	(54.66, 63.89)
5	(55.52, 65.23)	(55.52, 65.19)	(55.51, 65.07)
6	(55.54, 64.22)	(56.54, 64.19)	(56.55, 64.07)
7	(55.91, 63.66)	(55.91, 63.62)	(55.93, 63.50)
8	(55.07, 62.58)	(55.08, 62.55)	(55.10, 62.41)
9	(52.69, 60.15)	(52.70, 60.11)	(52.76, 59.95)

Rocket Position	9653	9654	9655
1	(62.11, 64.97)	(62.11, 64.96)	(62.11, 64.96)
2	(51.98, 64.24)	(51.98, 64.21)	(51.98, 64.17)
3	(53.66, 62.94)	(53.67, 62.91)	(53.67, 62.88)
4	(54.66, 63.87)	(54.67, 63.84)	(54.67, 63.82)
5	(55.51, 65.05)	(55.51, 65.02)	(55.51, 65.00)
6	(56.55, 64.06)	(56.55, 64.03)	(56.56, 64.01)
7	(55.93, 63.48)	(55.93, 63.46)	(55.94, 63.44)
8	(55.11, 62.39)	(55.12, 62.37)	(55.12, 62.34)
9	(52.77, 59.92)	(52.79, 59.89)	(52.80, 59.86)

Table 2, Continued

Rocket Position	Orbit No. 9656	9657	9658
1	(62.11, 64.94)	(62.11, 64.94)	(62.11, 64.93)
2	(51.99, 64.14)	(51.99, 64.10)	(51.99, 64.08)
3	(53.68, 62.85)	(53.68, 62.82)	(53.69, 62.80)
4	(54.67, 63.79)	(54.67, 63.76)	(54.67, 63.74)
5	(55.51, 64.97)	(55.51, 64.95)	(55.51, 64.93)
6	(56.56, 63.99)	(56.56, 63.97)	(56.56, 63.95)
7	(55.94, 63.41)	(55.94, 63.39)	(55.95, 63.37)
8	(55.13, 62.31)	(55.13, 62.29)	(55.14, 62.27)
9	(52.81, 59.82)	(52.83, 59.79)	(52.83, 59.77)

Rocket Position	9659	9661
1	(62.11, 64.93)	(62.11, 64.91)
2	(51.99, 64.08)	(51.99, 64.00)
3	(53.69, 62.80)	(53.70, 62.73)
4	(54.67, 63.74)	(54.68, 63.68)
5	(55.51, 64.93)	(55.50, 64.87)
6	(56.56, 63.95)	(56.56, 63.90)
7	(55.95, 63.37)	(55.95, 63.31)
8	(55.14, 62.27)	(55.15, 62.21)
9	(52.83, 59.77)	(52.87, 59.69)

Rocket Position	9657	9659	9661
10	(43.74, 70.42)	(43.73, 70.38)	(73.61, 44.29)
11	(40.59, 73.19)	(40.58, 73.15)	(40.52, 72.99)
12	(41.68, 74.42)	(41.66, 74.38)	(41.60, 74.23)
13	(41.08, 74.95)	(41.06, 74.91)	(40.99, 74.76)
14	(40.68, 74.50)	(40.66, 74.46)	(40.60, 74.30)
15	(41.80, 73.36)	(41.78, 73.31)	(41.73, 73.16)
16	(39.48, 75.56)	(39.46, 75.51)	(39.39, 75.35)

TABLE 3

Atomic Data

Ion	Line Energy (keV)	Wavelength (Å)	Element Abundance (N_Z/N_H)	Oscillator Strength
Fe IX	.0719	171.075	4.5×10^{-4}	3.72
Fe XI	.0653	188.22	4.5×10^{-4}	.075
Fe XII	.0630	195.138	4.5×10^{-4}	2.37
Fe XIII	.0603	203.84	4.5×10^{-4}	2.34
Fe XVII	.8257	15.013	4.5×10^{-4}	2.2
O VII	.5738	21.60	5.6×10^{-4}	.69
O VIII	.6535	18.97	5.6×10^{-4}	.42
Ne IX	.9218	13.45	3.5×10^{-5}	.72